Effect of Autoclaved Aerated Concrete on Dynamic Response of Concrete Gravity Dam Under Earthquakes

Fei Zhao, Shaoyu Zhao, and Shuli Fan

Abstract Autoclaved Aerated Concrete (AAC) is commonly used in lower floors buildings in low seismicity areas due to its lightweight property and high energy absorption capacity. This paper proposes a novel application of AAC as an effective seismic countermeasure in the reduction of vibrational energy for concrete gravity dam. According the vibrating characteristics and failure modes of gravity dam under earthquake excitation, AAC was placed in the upper zone of a gravity dam to reduce the seismic inertia force and consequently to increase the seismic safety of the dam. Dynamic responses of two non-overflow sections of a gravity dam were analyzed through finite element analysis utilizing a damaged plasticity constitutive model. The anti-seismic effect of using AAC in gravity dams is researched by inputting different kind of ground motion records. The comparison of the natural vibration characteristics, dam crest displacement, and dynamic damage of the dam were investigated. The results show that, AAC effectively improves seismic resistance of concrete gravity dams, particularly eliminating cracks in the concrete along reduced damage zones, through inertial force reduction and energy dissipation. The results warrant further considerations for applying AAC to gravity dams.

Keywords Autoclaved Aerated Concrete (AAC) · Concrete Gravity Dam · Earthquake · Mitigation of Earthquake Damage · Seismic Analysis

F. Zhao
National Disaster Reduction Center of China, Beijing 100124, China

S. Zhao
School of Civil Engineering, The University of Queensland, St. Lucia, QLD 4072, Australia

S. Zhao · S. Fan (✉)
State Key Laboratory of Coastal and Offshore Engineering, Dalian University of Technology, Dalian 116024, Liaoning, China
e-mail: shuli@dlut.edu.cn

G. Feng (ed.), *Proceedings of the 9th International Conference on Civil Engineering*,
Lecture Notes in Civil Engineering 327,
https://doi.org/10.1007/978-981-99-2532-2_35

1 Introduction

Nearly 70% of the national total hydropower potential is concentrated in the southwest region of China which region is well known for its high seismic intensity. With strong earthquakes predicted to occur in the coming decades, enhancing the seismic capacity of a high dam is of great concern. For concrete gravity dams or Roller Compacted Concrete (RCC) gravity dams higher than 100 m, real accidents, shaking table experiments and numerical simulation results indicate that the downstream face with an abrupt slope change is the weakest point during a strong earthquake. The best known case is the 103 m high Koyna dam in India which was seriously damaged during the 1967 earthquake [1]. The largest damages were the horizontal cracks on both the upstream and the downstream surfaces of several monoliths. Other gravity dams that experienced strong earthquakes, such as the Hsingfengkiang dam, China, and Sefid-Rud dam, Iran, also experienced the similar failure modes. Experiments on small scale models [2–4] and numerical simulations [5–7] have effectively rendered the dynamic responses and failure mechanism of concrete gravity dams during seismic excitation [8]. All these researches illustrate that the upper region with abrupt slope changes will be damaged seriously during earthquake and the neck position of a concrete gravity dam is the most vulnerable to a strong earthquake.

Adding steel reinforcement in potential cracking zones is a common remedial measure to enhance the seismic performance of gravity dams. Long et al. [9] performed numerical analyses to evaluate the effect of the reinforcement on the seismic damage of a 160 m high gravity dam using a modified embedded-steel model. Wang et al. [10] conducted a series of experiments on a shaking table to investigate the dynamic damage reaction of RCC gravity dam with and without reinforcements. These works indicate that the steel reinforcement in dam improves the seismic resistance of gravity dam and limits the possible rapid cracks expansion throughout a dam structure. Installing post-tensioned anchors in dams is another widely-used method to enhance their stability and to control prospective failure paths. Leger and Mahyari [11] carried out the numerical studies of post-tensioning pre-stressed cable seismic strengthening of concrete gravity dams. Morin et al. [12] studied the global seismic response of a post-tensioned gravity dam model. Ghaemmaghami and Ghaemian [13], with the help of a shaking table, tested a model dam after being repaired and strengthened using epoxy grouting of cracks and the installation of post-tensioned anchors. However, these seismic measures require a great deal of steel and are cost-intensive to prevent seismic cracking in gravity dams for the reason that a large amount of steel bars will be consumed in mass concrete dam section to satisfy the needs of the seismic performance [14]. In the meantime, the application of reinforced steel bar will result in long construction period and notable difficulty in the construction and quality control of roller compared concrete. Other methods, such as placing air-cushion insulation [15] and bonding fiber-reinforced polymer materials [16] to dam surface to increase energy dissipation, are also costly.

Autoclaved aerated concrete (AAC) is a mixture cementitious product of quicklime, water and sand, whose low density is formed by the existence of air bubbles in

the mixture. The prominent advantages of AAC are its lightweight and high energy absorption capacity, which economize the design of bracing structures including the foundation and walls of lower floors and reduce the seismic inertial force of structures [17]. Experiments were carried out in Europe and the U.S. to evaluate the seismic behavior of AAC type of masonry [18–21]. Varela et al. [22] made a suite of seismic tests of AAC shearwall specimens and developed a rational procedure to determine seismic performance factors for the design of AAC structures. Based on the experimentally observed responses, the hysteretic characteristics and the maximum drift ratio of 1% were proposed to avoid collapse of AAC structures. Imran and Aryanto [23] observed that AAC blocks exhibited better seismic performance than conventional clay-brick masonry under cyclic loading. Costa et al. [24] carried out experiments and nonlinear analyses of AAC infill structures to obtain a reliable and authentic depiction of the lateral cyclic behavior of AAC masonry buildings. The AAC masonry panel displays the apparent displacement ductility capacity and the maximum ultimate drift for panels failing in flexure is up to 0.5%. Ferretti et al. [25, 26] performed several tests on AAC masonry and beams to obtain a complete and integrated characteristic of AAC masonry behavior with attention to the softening regime and to describe AAC masonry behavior under different loading regime, determining some useful and essential parameters and values of AAC masonry. Bose and Rai [27] tested the resistance properties and hysteretic behavior of a single-reinforced concrete frame with AAC infill masonry. The test results showed that AAC infill at lower story drifts undertook the majority of the lateral load. The frame with AAC infill was found the first crack in the infill panel. At same time boundary separation cracking appeared between the AAC infill and top beam. The significant damage induced in AAC infill contributed to the energy dissipation and hysteretic damping. These researches reveal that AAC has the characteristic of a good combination of mechanical strength and energy dissipation, making it applicable for the implement of shear walls in seismic zones. It is beneficial for reinforced frame buildings to improve the seismic response by infilling AAC masonry in the upper stories.

In this paper, considering the advantages of light weight and strong energy dissipation capacity of AAC, we conducted a series detailed studies on the feasibility and suitability of AAC used in gravity dam as a shock and vibration mitigation measure. AAC infills were implemented in a gravity dam to replace a part of RCC to decrease the weight of the upper dam and to reduce its earthquake inertial forces and vibration energy. Nonlinear numerical analyses were carried out to investigate the dynamic damage of two non-overflow sections with heights 102 m and 189 m with the consideration of vibrational energy dissipation brought by AAC under different earthquake excitation.

2 Materials and Methods

2.1 Plastic-Damage Constitutive Model

The concrete damaged plasticity model implemented in the software ABAQUS was based on the constitutive relationships proposed by Lublinear et al. [28]. To simulate cracking and crushing of concrete under dynamic or cyclic loadings, this model was later amended by Lee and Fenves [6]. Based on basic damage mechanics, the effective stress $\overline{\sigma}_{ij}$ is defined as:

$$\overline{\sigma}_{ij} = E^0_{ijkl} : \left(\varepsilon_{kl} - \varepsilon^p_{kl}\right) \tag{1}$$

where E^0_{ijkl} is the initial elastic stiffness tensor, ε_{kl} and ε^p_{kl} are the elastic strain tensor and plastic strain tensor, respectively.

Concrete experiences damage when the stress level reaches the failure stress. The damage causes the softening of concrete material stiffness. Considering that concrete destruction is mainly caused by tensile damage, only the role of tensile damage was considered in this paper. The damage can be expressed by the damage factor d. Accordingly, the relationship of Cauchy stress σ_{ij} and effective stress $\overline{\sigma}_{ij}$ is defined by:

$$\sigma_{ij} = (1-d)\overline{\sigma}_{ij} = (1-d)E^0_{ijkl} : \left(\varepsilon_{kl} - \varepsilon^p_{kl}\right) \tag{2}$$

The plastic flow potential function and yield surface make use of two stress invariants of the effective stress tensor, namely the hydrostatic pressure stress $\overline{p}$,

$$\overline{p} = -\frac{1}{3\overline{\sigma}_{ij}} : I \tag{3}$$

and the Mises equivalent effective stress $\overline{q}$,

$$\overline{q} = \sqrt{3/2\left(\overline{S}_{ij} : \overline{S}_{ij}\right)} \tag{4}$$

where $\overline{S}_{ij}$ is the effective stress deviator, defined as

$$\overline{S}_{ij} = \overline{\sigma}_{ij} + \overline{p}I \tag{5}$$

As for as effective stresses, the yield function equation takes the following form:

$$F = \frac{1}{1-\alpha}\left(\bar{q} - 3\alpha\bar{p} + \beta\left(\varepsilon^p\right)\left\langle\hat{\bar{\sigma}}_{\max}\right\rangle - \gamma\left\langle-\hat{\bar{\sigma}}_{\max}\right\rangle\right) - \bar{\sigma}_c\left(\varepsilon^p_c\right) = 0 \tag{6}$$

$$\gamma = \frac{3(1-K_c)}{2K_c - 1} \tag{7}$$

where α and β are dimensionless material constants, $\widehat{\overline{\sigma}}_{\max}$ is the maximum principal effective stress, K_c is the strength ratio of concrete under equal biaxial compression to triaxial compression, and $\overline{\sigma}_c\left(\varepsilon_c^p\right)$ is the effective compressive cohesion stress.

The concrete damage plasticity model presumes non-associated potential plastic flow,

$$\dot{\varepsilon}_{ij}^p = \dot{\lambda}\frac{\partial G\left(\overline{\sigma}_{ij}\right)}{\partial \overline{\sigma}_{ij}} \tag{8}$$

The flow potential G used for this model is the Drucker-Prager hyperbolic function:

$$G = \sqrt{(\in \sigma_{t0}\tan\psi)^2 + \overline{q}^2} - \overline{p}\tan\psi \tag{9}$$

where $\psi(\theta, f_i)$ is the dilation angle measured in the $p - q$ plane at high confining pressure, σ_{t0} is the uniaxial tensile stress at failure, and $\in$ is a parameter, referred to as the eccentricity, that defines the rate at which the function approaches the asymptote.

2.2 Stress–Strain Laws in Uniaxial Tension of AAC

Performance of AAC infill was gauged by Imran and Aryanto [23] from the strength and deformation characteristics, the observed hysteretic energy dissipation capacity and the measured ductility through a series tests. However, the investigation on the stress–strain relationship and on constitutive mode of AAC under axial load, simulating seismic forces, is still limited. Few research provided a complete description of AAC masonry nonlinear fracture behavior [25, 29, 30], including inelastic parameters governing plastic stress–strain relationship. The AAC used in this paper is supplied by Dalian Tangjia Modern Building Material Co., LTD. The density ρ is 550 kg/m^3, the average compressive strength f_c is 3.1 MPa, and the elastic modulus E is 1320 MPa. For the experimental condition limitation, tensile strength and Poisson's ratio were not obtained. The direct tensile strength $f_{ct} = 0.54$ MPa, and the Poisson's ratio $\gamma = 0.38$ were found in the reference [25] for the reason that the density, compressive strength and the modules of the AAC are similar to those in this reference. The tensile properties of AAC are shown in Fig. 1.

3 Model Description and Design for Reducing Vibration

The Huangdeng gravity dam was selected in this paper. The dam is located on the upstream of Lancang River in Yunnan Province of China. Two typical non-overflow sections were selected for analysis, as shown in Fig. 2: Section A is a typical right

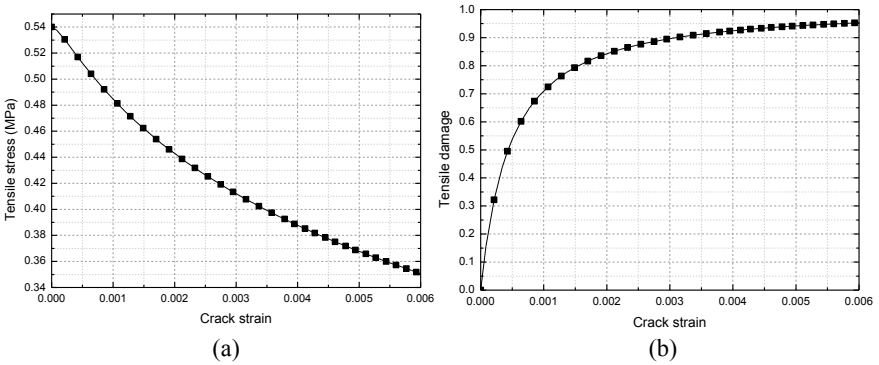

Fig. 1 AAC Tensile properties: **a** tensile stiffening; **b** tension damage

bank monolith 102 m tall with a 97 m deep reservoir, and Section B is a typical left bank monolith 189 m tall with a 184 m deep reservoir.

As mentioned above, cracks generally appear in the upper part of a gravity dam body during a seismic event, as it suffers from a whipping effect under earthquake excitation due to the sudden change of structural stiffness at the top of gravity dam. The acceleration at the crest of a gravity dam is 6 to 10 times that experienced at the dam heel [10, 31]. Thus, reducing the large inertial force in the upper part of a gravity dam is an effective method to decrease the damage sustained by a gravity dam during an earthquake. According the envelopes of maximum and minimum principal stresses for linear dynamic analysis of gravity dams [32], the middle region

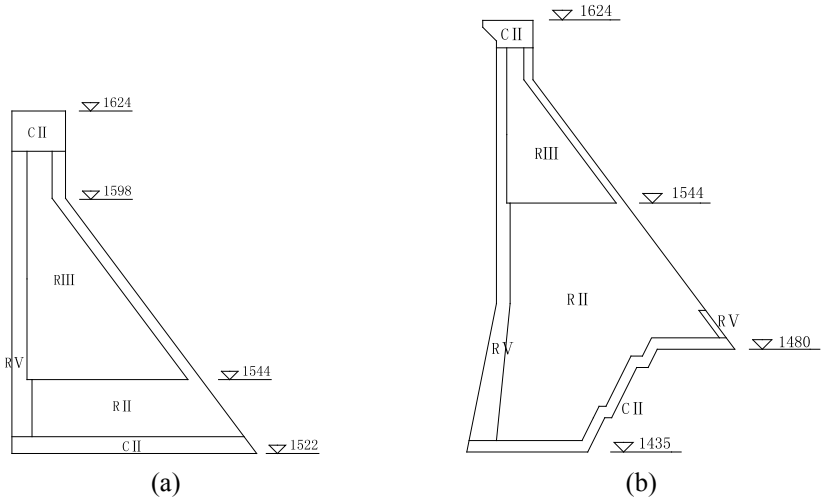

Fig. 2 Geometry and material partitions of two gravity dam sections: **a** Section A: the typical profile of right bank monolith; **b** Section B: the typical profile of left bank monolith

in the monolith is in low stress state, the larger tensile and compressive stresses just distribute at the surface of upstream and downstream. Therefore, low strength concrete can be used in the middle zones. And even these regions are designed to be empty, such as in the case of hollow gravity dam. Based on this characteristic, the authors first proposed the idea that AAC may be used in gravity dam as a seismic countermeasure to decrease the mass of the upper part. As a result, the inertial force of the upper part under earthquake excitation will be decreased. As shown in Fig. 2, the RIII partitions of the RCC dam were designed using low strength RCC. In this paper RCC in these zones were replaced by AAC in the new designed dam (named AAC dam) as a seismic countermeasure.

The plane stress conditions were assumed to conduct two-dimensional analyses of the non-overflow monolith. A finite foundation model was utilized and the finite foundations were extended three times the heights of the selected dam sections both in upstream, downstream and downwards directions. Considering energy dissipation resulted from the radiation damping at the far field and eliminating the effect of wave reflecting on artificial boundary, infinite elements were utilized at the boundaries of the finite foundation. The dam and the part of foundation which was in 20 m far away from the dam base were regarded as plastic-damage material. The partitions of dam concrete material were shown in Fig. 2. The mechanical parameters of materials were listed in Table 1. A dynamic amplification factor of 1.3 is took into account for the tensile and compressive strength to explain strain rate effects.

With the given dynamic tension softening curve and elastic properties of concrete and rock foundation, nonlinear dynamic analyses of damage development procedure in the gravity dam were conducted for different values of Peak Ground Acceleration (PGA). According the Specifications for Seismic Design of Hydraulic Structures in China (DL 5073-2000), three actual strong ground motion records at least should be used to research the failure mode of a hydraulic structure and evaluate its safety under earthquake excitation. In this paper, three typical ground motions recorded in the site of Class II were selected and applied in the stream and vertical direction of the dam-foundation system by taking account of duration, frequency characteristic and peak index of energy distribution. The typical strong ground motions are the records of Dec. 11, 1967 Koyna earthquake, the Taft record of the Kern County earthquake which was obtained on July 21, 1952 Kern county, California and the Qianan record which was obtained in Tangshan aftershock occurs on Aug. 9, 1976. The records

Table 1 The material mechanics parameters of dam and bedrock

Material partition	CII	RII, RV	RIII	AAC	Bedrock
Dynamic elastic modulus (MPa)	33,150	33,150	28,600	1716	8000
Poisson ratio	0.167	0.167	0.167	0.38	0.25
Density (kg/m^3)	2400	2400	2400	550	2610
Static compressive strength (MPa)	13.2	13.2	9.9	3.1	30
Dynamic compressive strength (MPa)	17.16	17.16	12.87	4.03	45
Dynamic tensile strength (MPa)	1.72	1.72	1.287	0.54	1.5

of these ground motions were given in Fig. 3. Keeping the same waveform, the amplitude of the acceleration time histories was increased step by step until the crack propagated through the dam. The PGA of Koyna horizontal record was adjusted to 502 gal for Section A as the exciting load, and 402 gal for Section B. The PGA of Taft record and Qianan record are 176 gal and 351 gal for Section A, respectively. The vertical earthquake acceleration representative value is two-thirds of the horizontal acceleration representative value according the provisions of DL 5073-2000. The dynamic analysis of the dam-foundation system was conducted considering the static analysis results as the initial conditions including gravity loads and hydrostatic loads.

The hydrodynamic effect of reservoir water was modelled using the method of additional mass [33]. The additional mass per unit area of the upstream wall was given in approximate form by the expression:

$$P_w(y) = \frac{7}{8}\rho_w\sqrt{h_w(h_w - y)}, \quad \mathrm{y} \le h_w \tag{10}$$

where $\rho_w = 1000$ kg/m^3 is the density of water, h_w is the depth of water, and y is the height from water surface to the location. It is assumed that the hydrodynamic pressures derived from the vertical ground acceleration component are neglected in all the numerical analysis for the reason that they are small.

4 Seismic Analysis

4.1 Dynamic Characteristics of Different Dam Sections

At first the changes on the dynamic characteristics of the selected dam sections were investigated. The first twenty natural frequencies of the AAC dam and RCC dam were shown in Fig. 4 and the first five frequencies were list in Table 2.

Since stiffness and mass changes simultaneously, the different order frequencies and different sections have an irregular rate of change. For section A, the first natural frequency of AAC dam is 1.56 Hz, decreasing 1.65% compared with that of RCC dam which is 1.58 Hz. However, the third natural frequency increases from 4.15 Hz to 4.21 Hz when the RCC in RIII district is replaced by AAC. As for Section B with 189 m height, the first natural vibration frequency of AAC dam is 1.03 Hz, which is 3% higher than that of RCC dam. All other frequencies decrease after the RCC is replaced by AAC in the upper part of Section B. The first three natural frequencies oscillate within a small amplitude that varies no more than 5% after RCC replaced by AAC in the RIII district of the selected sections. But for high frequencies, the vibration frequencies of AAC dams reduce quickly for the reason that the elastic modulus of AAC is extremely small. The rate of change is more than 20%, especially for Section A with 102 m height. The mass participation factor of AAC dam in vertical direction decreases in the second mode and increases in the

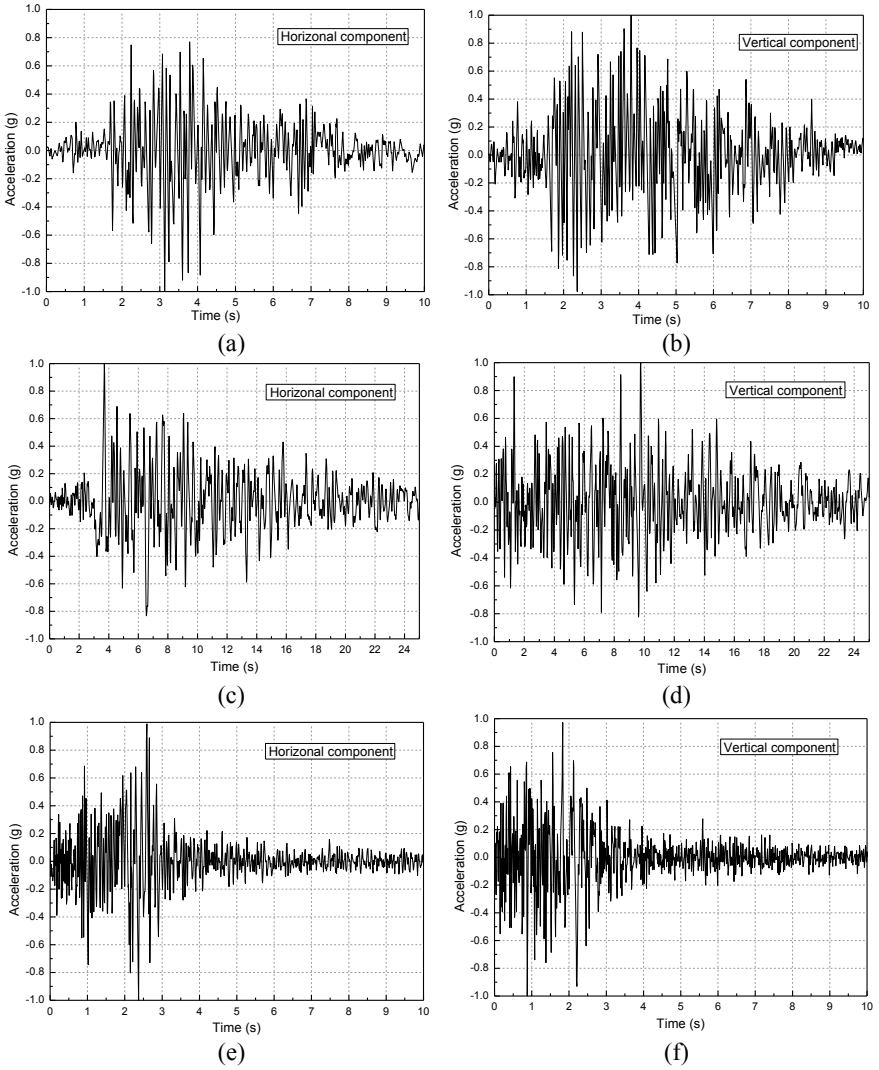

Fig. 3 The normalized acceleration: **a** Horizontal component of Koyna record; **b** Vertical component of Koyna record; **c** Horizontal component of Taft record; **d** Vertical component of Taft record; **e** Horizontal component of Qianan record; **f** Vertical component of Qianan record

third mode compared with the RCC dam, as shown in Table 3. Therefore, for the AAC dam, the first and second modes vibrate in the horizontal direction, and the third mode vibrates in the vertical direction.

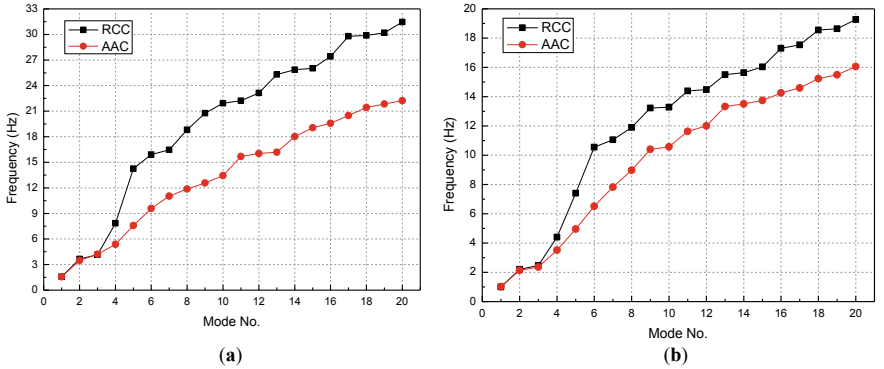

Fig. 4 Influence of AAC on the natural frequency of gravity dam: **a** Natural frequency of Section A: 102 m monolith; **b** Natural frequency of Section B: 189 m monolith

Table 2 The first five natural frequencies of gravity dam infilled with RCC and AAC

Mode No.	Section A			Section B		
	RCC dam (Hz)	AAC dam (Hz)	Change rate (%)	RCC dam (Hz)	AAC dam (Hz)	Change rate (%)
1	1.58	1.56	−1.65	1.00	1.03	3.05
2	3.65	3.49	−4.43	2.21	2.14	−3.13
3	4.15	4.21	1.34	2.47	2.36	−4.59
4	7.85	5.37	−31.53	4.40	3.52	−20.12
5	14.26	7.58	−46.81	7.41	4.96	−33.07

Table 3 The mass participation factors in x component and y component

Mode No.	Section A				Section B			
	RCC dam		AAC dam		RCC dam		AAC dam	
	X	Y	X	Y	X	Y	X	Y
1	0.75	0.02	0.66	0.01	0.76	0.02	0.72	0.02
2	0.08	0.85	0.21	0.0007	0.08	0.87	0.23	0.002
3	0.14	0.12	0.03	0.91	0.13	0.11	0.01	0.97
4	0.02	0.01	0.09	0.05	0.02	0.00	0.03	0.01
5	0.002	0.0005	0.01	0.0004	0.002	0.00001	0.01	0.0023

4.2 Time History Analysis of Displacement and Acceleration

The stream displacement time histories of the dam crest deviated from the values corresponding to static loads are shown in Fig. 5. The black line is the original dam response, whereas the red line is the response of the AAC dam. The positive

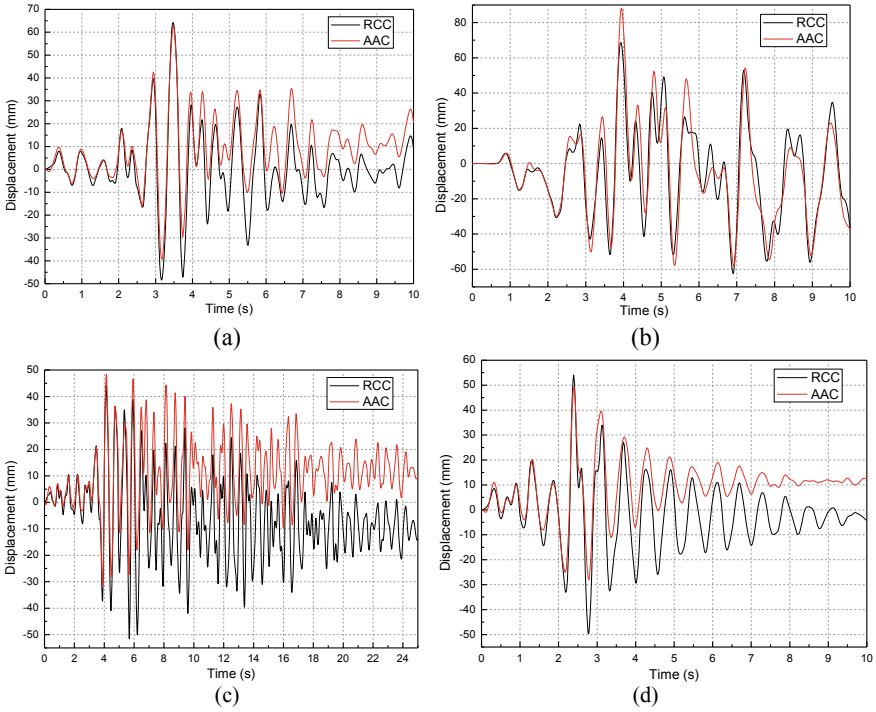

Fig. 5 Time history graphs of the horizontal displacement at the dam crest: **a** Displacement response of Section A (Koyna record); **b** Displacement response of Section B (Koyna record); **c** Displacement response of Section A (Taft record); **d** Displacement response of Section A (Qianan record)

direction of the horizontal displacement is in the stream direction. Comparing the curves, it can be found that the dynamic displacement response has less sensitivity on the replacing RCC by AAC. This means that the AAC infill has little effect on the dynamic deformation of the selected dam sections.

For the low gravity dam as Section A excited by Koyna record, the maximum dynamic displacement of AAC dam is 62.55 mm which occurred at 3.48 s, decreasing 1.64 mm compared with the results of the RCC dam, as shown in Fig. 5(a). A large deformation dam appears in AAC dam and the residual deformation at the dam crest is 20.36 mm at the end of the earthquake.

For Section B (height = 189 m), as shown in Fig. 5(b), the maximum displacement caused by the Koyna record increases from 68.62 mm to 88.32 mm as a result of the stiffness deterioration of structures when the RCC in RIII region is replaced by the AAC. Other than the increasing amplitudes at the peak points, there is only a slight difference in the horizontal displacement computed using AAC dam model and RCC dam model. The application of AAC has less effect on the dynamic deformation of a high gravity dam than that of a low gravity dam.

Comparing with the RCC dam, the first large dynamic displacement of AAC dam Section A in the stream direction increases from 43.93 mm to 48.33 mm at 4.13 s when the Taft record is applied in the structures. In Fig. 5(c) it can also be found that the reciprocating center axis of AAC dam is mainly concentrated in the 10 mm vicinity of downstream direction due to the long duration of the Taft record, which is different with the results of RCC dam. Residual deformation of AAC dam appears on the dam crest due to the light weight and low elastic modulus of AAC, which changes from −13.8 mm (upstream direction) to 10.48 mm (downstream direction) when the RCC in RIII region is replaced by AAC.

As shown in Fig. 5(d), the maximum displacement of AAC dam Section A in the stream direction is 49.35 mm which occurs at 2.40 s, decreasing 4.74 mm compared with that of the RCC dam when the dam section is subjected to Qianan record. After that time, the divarication emerges between the dynamic responses of RCC dam and AAC dam. The vibration range of AAC dam is smaller than that of RCC dam. The larger horizontal displacement appears the tendency to stream direction appears when the AAC is used in RIII partitions. At the end of earthquake, the residual deformation reaches 12.39 mm.

The horizontal acceleration time histories of dam crest for the RCC dam and the AAC dam due to the earthquake loads are shown in Fig. 6. When the lightweight material AAC is used, the amplitude of acceleration at dam crest oscillates with a slight change compared with that of RCC dam under different seismic motions despite the lighter upper part of the block. The most reason is that the three-first natural frequencies have small variation of amplitudes as mentioned above. And for a gravity dam, the first three natural frequencies play a dominant role in the dynamic response of gravity dam under seismic excitation. The replacement of RCC in RIII partitions by AAC does not change the acceleration response of gravity dam obviously. However, the density of concrete in upper part of gravity dam decreases from 2400 kg/m^3 to 550 kg/m^3. Therefore, the inertial force of the upper part will be reduced less than one quarter under the same earthquake excitation after RCC in RIII partitions is replaced by AAC.

4.3 Seismic Wave Effects on the Damage of the Dams

A strong earthquake often causes stiffness and strength deterioration of structures. In this section, the effects of AAC application on the dynamic damage response of the dam-reservoir-foundation system were investigated by comparison of the AAC dam and RCC dam dynamic solutions. The influence of upper block weight on the damage of gravity dam was researched to investigate the seismic performance of AAC with different spectral characteristics.

Figures 7 and 8 show the accumulated tensile damage profiles of the RCC dam and AAC dam Section A with different ground motions. A penetrating crack is found at the neck position of the RCC dam propagating from the downstream face to the upstream face at approximately a 45° angle to the vertical under the Koyna record

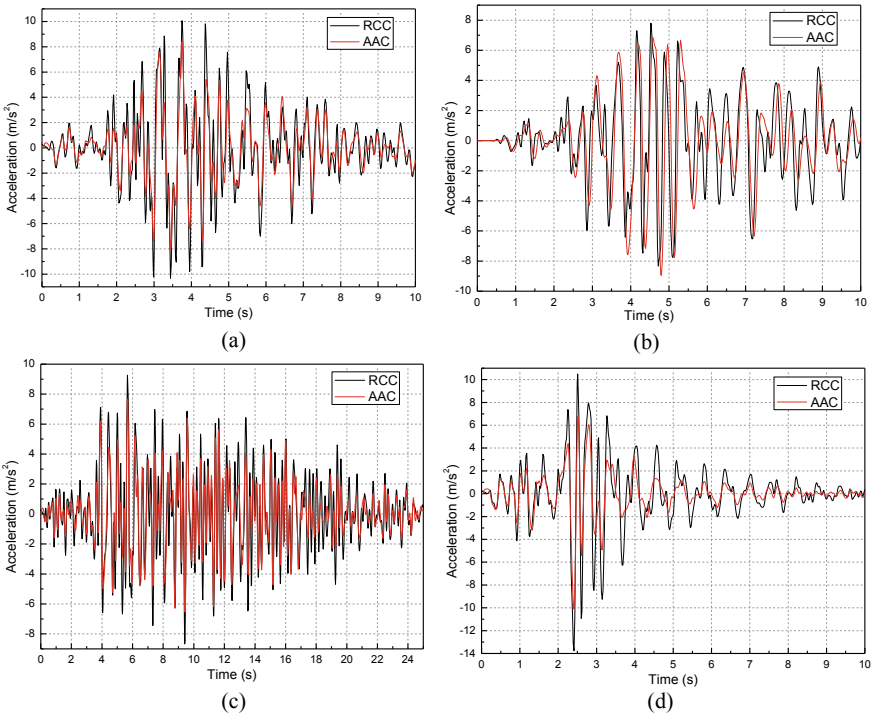

Fig. 6 Time history graphs of the horizontal acceleration at the dam crest: **a** Acceleration response of Section A (Koyna record); **b** Acceleration response of Section B (Koyna record); **c** Acceleration response of Section A (Taft record); **d** Acceleration response of Section A (Qianan record)

excitation, similar to the failure modes of the Koyna dam. At the same time, another crack appears at the heel of dam, however it propagates at approximately a 45° angle into the foundation, different with the damage profile reported in literatures [6, 32] which the foundation was assumed as a rigid body. As shown in Fig. 7(b) and (c), a similar damage profiles appear in the RCC dam Section A when the Taft record and Qianan record are applied in the low gravity dam section. However, the penetrating cracks at neck position appear a furcation in the interior of dam body, and more damage zones are found at the downstream surface under the Taft and Qianan records excitation.

For the AAC dam of Section A, damages are mainly concentrated in the dam heel and the contact layer of RCC and AAC at the upstream surface no matter which ground motion record is applied. The initial cracking profiles are nearly horizontal, and then extend into the foundation. The crack on the upstream surface extends into dam body about 4 m along the contact layer of RCC and AAC for the reason of stiffness deterioration. The cracking profiles of AAC dam in these two zones are more serious than those of RCC dam, as seen in the comparison of Fig. 7 and 8. The main reason is that the weight of the upper block of AAC dam is less than

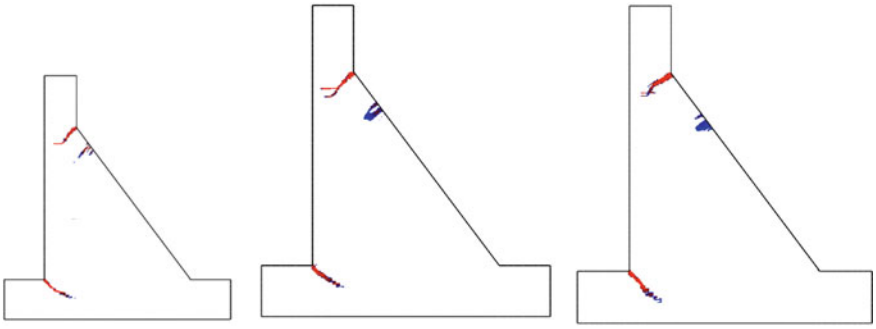

Fig. 7 Evolution of tensile damage of RCC dam Section A under different ground motion excitation

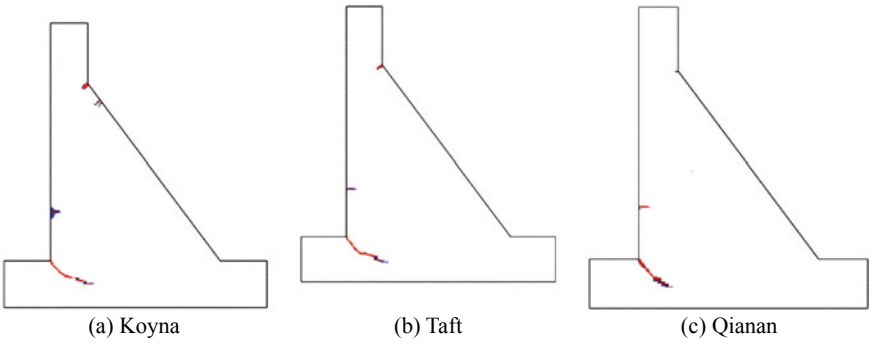

Fig. 8 Evolution of tensile damage of AAC dam Section A under different ground motion excitation

that of RCC dam. However, the throughout crack at the slope change at downstream disappears with the application of AAC. Thus it can be inferred that AAC application is effective in decreasing the dynamic response of gravity dam under different ground motions excitation, consequently inhibiting damage propagation through the energy dissipation due to the plastic deformation of AAC.

4.4 Dam Height Effects on Damage of the Dams

In this section, the seismic damage analyses of the high dam Section B subjected to the Koyna record were performed. The dynamic responses of RCC dam and AAC dam were examined to evaluate the effects of dam height on AAC seismic performance.

For the RCC dam of Section B, damages are mainly concentrated in the vicinity of discontinuity at the upstream and downstream surface in addition to the dam heel, as shown in Fig. 9. There are two cracks at the downstream surface. One crack extends

completely across the upper section. Due to the high compressive stress at the dam heel of the high dam section, there is less damage of Section B at dam heel than those of Section A. At the slope change of the upstream face, the crack almost propagates at a horizontal angle.

The damage propagations of AAC dam are different with those of RCC dam as shown in Fig. 9 and Fig. 10. No throughout crack occurs in the upper part of dam at the slope change for the AAC dam because of the light weight and the energy dissipation property of the AAC. However, as a tradeoff, the base crack propagates more in the case of AAC. There is another crack that appears at the upstream surface at the contact layer of AAC and RCC. These Figures show that the application of AAC in upper part helps to reduce the damage zone and retain the integrity of the dam's upper part, which is prone to cracking.

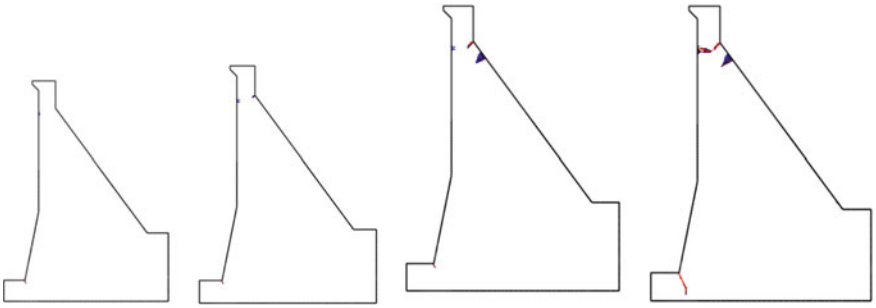

Fig. 9 Evolution of tensile damage of RCC dam Section B under Koyna record

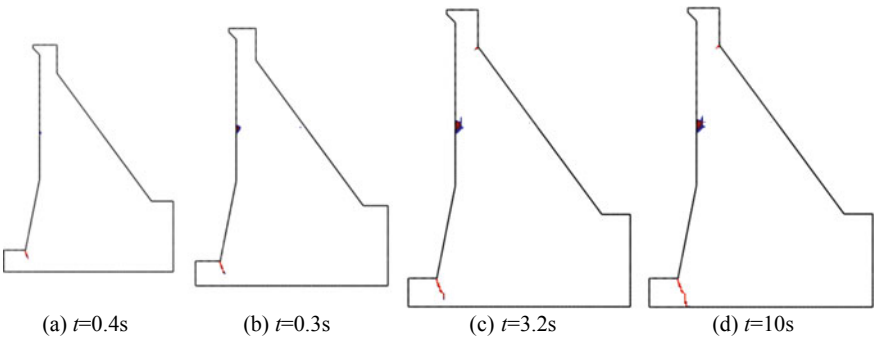

Fig. 10 Evolution of tensile damage of AAC dam Section B under Koyna record

4.5 Discussion of Results

The results mentioned above show that the horizontal displacement of RCC dam of section A oscillates with a shaft line. However, the displacement of AAC dam of section A basically increases and the oscillating axis shifts toward the downstream direction under different ground motions. Furthermore, earthquake duration has obvious influence on the displacement response of the gravity dam. Because of the high energy generated by the long duration of Taft record, displacement curves between AAC dam and RCC dam appear apparent separation at the time of approximately ten second of earthquake record.

In these numerical studies, the residual deformation at the crest of low gravity dam increases at the end of ground motions after the RCC in the upper part of gravity dam is replaced by AAC. There is a slight difference for high gravity dam in the dynamic deformation computed using AAC dam model and RCC dam model. Moreover, no matter how high the gravity dam is, the amplitude of acceleration at dam crest has a slight change between the RCC dam and AAC dam. So, it seems that AAC is more suitable to be used in high gravity dam to reduce the inertial force and vibrational energy.

The dynamic damage analyses of dams have shown that the weak parts of RCC gravity dam structures under seismic excitation is mainly concentrated in the vicinity of discontinuity at the upstream and downstream surface and the dam heel. However, the penetrating crack disappears at the neck position for AAC dam. It has been shown that the AAC plays a significant role of seismic response reduction and improves the seismic performance of the gravity dam body through energy dissipation. At same time the application of AAC leads to greater accumulate damage at the dam heel and the upstream surface at the contact layer of AAC and RCC, which calls for special aseismic design attention. Additional techniques should be used to guarantee sufficient strengthening for these locations. Optimizing studies on the location and region size of AAC should be further conducted to investigate the application of AAC in gravity dam as an aseismic measure for vibration reduction and damage mitigation.

5 Conclusions

This paper researched the feasibility of AAC as a seismic countermeasure to enhance the aseismic performance of gravity dams. The effect of AAC on the dynamic responses and failure modes of different height gravity dams under different ground motions was studied. Due to the lightweight and high energy absorption capacity of AAC material, the earthquake response of a gravity dam can be mitigated by replacing the RCC in upper low stress region to AAC. The application of AAC reduces the damage zone near the upper region with abrupt slope changes of the gravity dam sections. AAC is a suitable seismic countermeasure for improving the

seismic performance of gravity dam. However, the weight decrease leads to greater accumulated damages at the dam heel, which calls for special aseismic design attention. In authors' future work, additional optimizing analyses on the location and region size of AAC will be performed.

Acknowledgements This work was partially supported by the National Key Research and Development Program of China (Grant No. 2017YFC1503002). The authors would like to thank them for their financial support. Thank Mrs. Ing Lim for professional editing and English corrections.

References

1. Chopra A, Chakrabarti P (1973) The Koyna earthquake and the damage to Koyna dam. Bull Seismol Soc Am 63(2):381–397
2. Donlon WP, Hall JF (1991) Shaking table study of concrete gravity dam monoliths. Earthq Eng Struct Dyn 20(8):769–786
3. Harris DW, Snorteland N, Dolen T, Travers F (2000) Shaking table 2-D models of a concrete gravity dam. Earthq Eng Struct Dyn 29(6):769–787
4. Mridha S, Maity D (2014) Experimental investigation on nonlinear dynamic response of concrete gravity dam-reservoir system. Eng Struct 80:289–297
5. Bhattacharjee SS, Leger P (1993) Seismic cracking and energy dissipation in concrete gravity dams. Earthq Eng Struct Dyn 22(11):991–1007
6. Lee J, Fenves GL (1998) A plastic-damage concrete model for earthquake analysis of dams. Earthq Eng Struct Dyn 27(9):937–956
7. Tinawi R, Leger P, Leclerc M, Cipolla G (2000) Seismic safety of gravity dams: from snake table experiments to numerical analyses. J Struct Eng-ASCE 126(4):518–529
8. Wang G, Wang Y, Lu W, Zhou C, Chen M, Yan P (2015) XFEM based seismic potential failure mode analysis of concrete gravity dam-water-foundation systems through incremental dynamic analysis. Eng Struct 98:81–94
9. Long Y, Zhang C, Xu Y (2009) Nonlinear seismic analyses of a high gravity dam with and without the presence of reinforcement. Eng Struct 31(10):2486–2494
10. Wang M, Chen J, Fan S, Lv S (2014) Experimental study on high gravity dam strengthened with reinforcement for seismic resistance on shaking table. Struct Eng Mech 51(4):663–683
11. Leger P, Mayahari A (1994) Finite element analysis of post-tensioned gravity dams for floods and earthquakes. Dam Eng 5:5–27
12. Morin PB, Leger P, Tinawi R (2002) Seismic behavior of post-tensioned gravity dams: shake table experiments and numerical simulations. J Struct Eng 128(2):140–152
13. Ghaemmaghami AR, Ghaemian M (2010) Shaking table test on small-scale retrofitted model of Sefid-rud concrete buttress dam. Earthq Eng Struct Dyn 39(1):109–118
14. Hall JF, Dowling MJ, El-Aidi B (1992) Defensive earthquake design of concrete gravity dams. Dam Eng 3(4):249–263
15. Liu H, Zhang S, Chen J, Sun M, Sun L, Li Y (2011) Simulation analysis theory and experimental verification of air-cushion isolation control of high concrete dams. Sci China Technol Sci 54(11):2854–2868
16. Zhong H, Wang N, Lin G (2013) Seismic response of concrete gravity dam reinforced with FRP sheets on dam surface. Water Sci Eng 6(4):409–422
17. Narayanan N, Ramamurthy K (2000) Structure and properties of aerated concrete: a review. Cem Concr Compos 22(5):321–329
18. Tanner JE, Varela JL, Klingner RE, Brightman MJ, Cancino U (2005) Seismic testing of autoclaved aerated concrete shearwalls: a comprehensive review. ACI Struct J 102(3):374–382

19. Penna A, Magenes G, Calvi GM, Costa AA (2008) Seismic performance of AAC infill and bearing walls with different reinforcement solutions. In: Proceeding of the 14th international brick and block masonry conference, Sydney, Australia
20. Siddiqui UA, Sucuoglu H, Yakut A (2015) Seismic performance of gravity-load designed concrete frames infilled with low-strength masonry. Earthq Struct 8(1):19–35
21. Rosti A, Penna A, Rota M, Magenes G (2016) In-plane cyclic response of low-density AAC URM walls. Mater Struct 49(11):4785–4798
22. Varela JL, Tanner JE, Klingner RE (2006) Development of seismic force reduction and displacement amplification factors for autoclaved aerated concrete structures. Earthq Spectra 22(1):267–286
23. Imran I, Aryanto A (2009) Behavior of reinforced concrete frames in-filled with lightweight materials under seismic loads. Civ Eng Dimension 11(2):69–77
24. Costa AA, Penna A, Magenes G (2011) Seismic performance of autoclaved aerated concrete (AAC) masonry: from experimental testing of the in-plane capacity of walls to building response simulation. J Earthq Eng 15(1):1–31
25. Ferretti D, Michelini E, Rosati G (2015) Cracking in autoclaved aerated concrete: experimental investigation and XFEM modeling. Cem Concr Res 67:156–167
26. Ferretti D, Michelini E, Rosati G (2015) Mechanical characterization of autoclaved aerated concrete masonry subjected to in-plane loading: experimental investigation and FE modeling. Constr Build Mater 98:353–365
27. Bose S, Rai DC (2016) Lateral load behavior of an open-ground-story RC building with AAC infills in upper stories. Earthq Spectra 32(3):1653–1674
28. Lubliner J, Oliver J, Oller S, Onate E (1989) A plastic-damage model for concrete. Int J Solids Struct 25(3):299–326
29. Trunk B, Schober G, Helbing AK, Wittmann FH (1999) Fracture mechanics parameters of autoclaved aerated concrete. Cem Concr Res 29(6):855–859
30. Yang K, Lee K (2015) Tests on high-performance aerated concrete with a lower density. Constr Build Mater 74:109–117
31. Chen J, Wang M, Fan S (2013) Experimental investigation of small-scaled model for powerhouse dam section on shaking table. Struct Control Health Monit 20(5):740–752
32. Calayir Y, Karaton M (2005) Seismic fracture analysis of concrete gravity dams including dam-reservoir interaction. Comput Struct 83(19):1595–1606
33. Westergaard H (1933) Water pressure on dams during earthquake. Trans ASCE 98(2):418–472